



Morphologically different hydroxyapatite nanoparticles exert differential genotoxic effects in *Drosophila*

Merve Güneş ^a, Burçin Yalçın ^a, Ayşen Yağmur Burgazlı ^a, Ghada Tagorti ^a, Emre Yavuz ^b, Esin Akarsu ^b, Nuray Kaya ^a, Ricard Marcos ^{c,*}, Bülent Kaya ^{a,*}

^a Department of Biology, Faculty of Sciences, Akdeniz University, Antalya, Turkey

^b Department of Chemistry, Faculty of Sciences, Akdeniz University, Antalya, Turkey

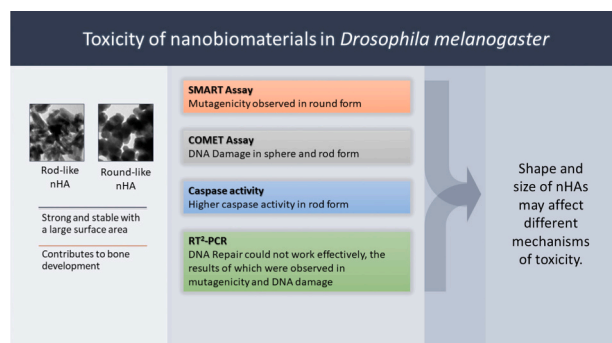
^c Department of Genetics and Microbiology, Universitat Autònoma de Barcelona, Cerdanyola del Vallès, Spain



HIGHLIGHTS

- Shape and size of hydroxyapatite nanoparticles (HAP-NPs) modulate hazardous effects.
- The toxic effects of spherical HAP-NPs were higher than those of the rod form.
- HAP-NPs may have potential apoptotic effects.
- DNA repair pathways were affected by exposure to HAP-NPs.

GRAPHICAL ABSTRACT



ARTICLE INFO

Editor: Damia Barcelo

Keywords:

Caspase
Drosophila melanogaster
Single-cell gel electrophoresis
Somatic mutation and recombination
DNA repair
Gene expression

ABSTRACT

Hydroxyapatite (HAP) occurs naturally in sedimentary and metamorphic rocks and constitutes the hard structures in many organisms. Since synthetic nano-sized HAP (HAP-NPs) are used in orthopedic applications and for heavy metal remediation in aquatic and terrestrial media, both environment and humans are exposed to them. Due to the concerns about their potential hazards, the genotoxic effects that round/rod forms of HAP-NPs were investigated in *Drosophila* using the wing-spot and the comet assays. Furthermore, caspase activities were evaluated to examine the activation of cell death pathways. As a novelty, the expression of 36 genes involved in DNA repair was investigated, as a tool to indirectly determine DNA damage induction. Obtained sizes were 35–60 nm (roundHAP-NPs) and 45–90 nm (rodHAP-NPs) with a low Zeta-potential (−1.65 and 0.37 mV, respectively). Genotoxicity was detected in the wing-spot (round form), and in the comet assay (round and rod-like HA-NPs). In addition, increased expression of Caspases 3/7, 8, and 9 activities were observed. For both HAP forms, increased changes in the expression were observed for mismatch repair genes, while decreased expression was observed for genes involved in ATM, ATR, and cell cycle pathways. The observed changes in the repair pathways would reinforce the view that HAP-NPs have genotoxic potential, although more markedly in the round form. Thus, the environmental presence of engineered nanoparticles, including HAPs, raises concerns

* Corresponding authors.

E-mail addresses: ricard.marcos@uab.es (R. Marcos), bkaya@aldeniz.edu.tr (B. Kaya).

about potential effects on human health. It is essential that the effects of their use are carefully assessed and monitored to ensure safety and to mitigate any potential adverse effects.

1. Introduction

Biomaterials are compounds used to increase body functions and/or to replace damaged tissues which have played a relevant role in transforming medicine over the last few decades (Montoya et al., 2021). In this context, calcium phosphate-based biomaterials are widely used for repairing bone defects, due to their similarities to the inorganic components of human bones. Among them, hydroxyapatite (HAP) stands out (Filip et al., 2022). Besides its therapeutic uses, HAP has many other ones such as removing heavy metal pollution from aquatic and terrestrial systems and wastewater (Brazdis et al., 2021). Composites created with HAP are used as environmentally friendly cleaners for paint removal from wastewater (Pai et al., 2021). Thus, among the potential materials for fluoride removal, HAP and HAP-based composites stand out with excellent performance at neutral and near-neutral pH (Rathnayake et al., 2022). Furthermore, Since HAP is soluble in the acidic environment of the stomach, the dissolved ions reach the intestine similarly to other calcium sources and for this reason, they are proposed to be used as food additives (Enax et al., 2022).

It is important to remark that HAPs are naturally found either in mammals (bone structures), aquatic organisms (spines and shells), plants, and algae, as well as in limestone minerals (Mohd Pu'ad et al., 2019; Kalpana and Nagalakshmi, 2023). Since the production of HAP in nano-size is synthetically feasible, their applications in various fields, particularly medicine, is steadily growing. Nevertheless, there is limited data on the potential toxicity of HAP (Righi et al., 2023).

Nanotechnology permits the molecular design and production of materials in the nano-range controlling size, morphology, and other physicochemical properties (Ignjatovic et al., 2020). Specifically, nanotechnology permits to obtain biomaterials of increasing biocompatibility by controlling their structural properties, such as pore volume, shape, diameter, and solubility (Bonilla-Represa et al., 2020). Thus, compared to conventional ceramic formulations, the nanoparticles of apatite (HAP-NPs) present characteristics such as surface particle size and pore size more efficient in their interactions with other molecules.

As for the other nanomaterials, the potential hazards associated to the use of HAP-NPs have been pointed out. A recent review did not find associated hazards (Zaffarin et al., 2021), confirming the previous reported for nanoscopic calcium phosphate (Epple, 2018). Nevertheless, in exposed Wistar rats (300 mg/kg bw for 45 days) HAP-NPs reduced the levels of stomach antioxidant enzymes as well as glutathione (Mosa et al., 2020). In addition, round and rod-shaped HAP-NPs delayed embryo hatching in zebrafish (3–100 µg/mL for 7–2 h) (Zhao et al., 2013), which would agree with data reporting that some nanomaterials properties, such as shape and size, influence the toxicological profile of nanomaterials (Dong et al., 2019). Accordingly, further studies on the hazardous effects of HAP-NPs, considering shape characteristics are required.

The aim of this study was to evaluate the potential toxicity of two different forms of HAP-NPs in *D. melanogaster* using different toxicity assays. For such purpose, two different HAP-NPs shapes were synthesized, namely round and nanorods HAP-NPs. To determine their potential hazardous effects, *Drosophila* was used as a model organism, which was reported to present many advantages when testing nanomaterials (Alaraby et al., 2016). Furthermore, considering the metabolic similarities of *Drosophila* with mammals (dietary inputs including nutrient intake-digestion-absorption-storage, xenobiotic metabolism system, antioxidant enzymes and DNA replication and repair systems), it seems that this model organism can be successfully used to investigate the genotoxic potential of different agents (Mishra et al., 2017; Furlanetto et al., 2018; Naves et al., 2018). In addition to the classical

approaches to detect genotoxicity, such as the detection of somatic mutation and recombination and the detection of DNA breaks (comet assay), toxicogenomic tools have also been used. This approach, using high-performance omics technologies, analyze and interpret changes in gene expression resulting from exposure to genotoxins. Molecular profiling methods, including bioinformatics techniques, permit the simultaneous analysis of a multitude of gene variants to search for genes prone to damage, detecting patterns and mechanisms of genotoxicity, and identifying specific gene expression profiles that can provide biomarkers of exposure and risk (Portugal et al., 2022). (Portugal et al., 2022). The used toxicogenomic tools will help to understand the genotoxicity data obtained in standard assays, showing the way of how future genotoxicity studies should be carried out. Our final goal is to comprehensively investigate the genotoxic effects of HAP-NPs in *Drosophila*, as a suitable *in vivo* model, to assess the safety of these materials.

2. Materials and methods

2.1. Chemicals

Calcium nitrate tetrahydrate [Ca(NO₃)₂·4H₂O], ammonium dihydrogen phosphate [NH₄H₂PO₄], diammonium dihydrogen phosphate [(NH₄)₂HPO₄], ortho-phosphoric acid, propionic acid, Arabic gum, chloral hydrate, glycerol, sodium hydroxide (NaOH), ethylenediamine tetra acetic acid (Na₂EDTA), sodium chloride (NaCl), Trizma Base Bio-Ultra, sodium hydroxide (NaOH), ethidium bromide (EtBr), phosphate buffer (PBS), phenylthiourea, Triton-X, sarcosine, Tris HCl, Na₂H₂P₂O₇, β-glycerophosphate, and Coomassie Blue were purchased from Sigma Aldrich (Saint Louis, MO, USA). Low melting agar, and low melting agar (DNA grade) were purchased from AppliChem (Darmstadt, Germany). All chemicals were used in their analytical grade, without further purification.

2.2. Synthesis of nano hydroxyapatite

Various approaches such as sol-gel, hydrothermal, co-precipitation, wet/dry and mechanical-chemical reactions can be used to synthesize HAP (Bonilla-Represa et al., 2020; Osuchukwu et al., 2021; Venkatesan and Anil, 2021). Considering the advantages of each one of the methods, it is also possible to combine processes for HAP synthesis. Among them, the ionic mixing of calcium and phosphorus in the sol-gel method has provided a specific microstructure and superior physical and chemical homogeneity (Panda et al., 2021); accordingly, this synthesis approach was used in our study.

2.3. Round form of nano hydroxyapatite

Round-like hydroxyapatite nanoparticles (roundHAP-NPs) were synthesized according to our previous study (Yavuz et al., 2021). The reaction was carried out by keeping the atomic ratio 1.67 for Ca/P. Firstly, 78.88 g of Ca(NO₃)₂·4H₂O and 129.6 mL of ethanol were stirred until they became a homogeneous solution. Then, the pH of the solution was set at 10 by adding NH₃. Afterwards, 23.2 g of NH₄H₂PO₄ and 186.5 mL of distilled water were stirred to gain a homogenous phosphate solution. Following this, the pH of the solution was set at 10 by adding NH₃. Next, the calcium solution was added (2.4 g/min) over a stirring phosphate solution. The resulting solution was kept for 22 h at room temperature and centrifuged at 5000 rpm for 5 min. Finally, the obtained HAP particles were washed six times with distilled water and dried under vacuum at 70 °C for 24 h. After that, HAP-NPs particles were calcined at 750 °C for 4 h.

2.4. Rod form of nano hydroxyapatite

Rod-like hydroxyapatite particles (rodHAP-NPs) were produced using a modified chemical precipitation technique setting the atomic ratio to 1.67 for Ca/P (Nagyné-Kovacs et al., 2018). Briefly, 17.712 g of $\text{Ca}(\text{NO}_3)_2 \cdot 4\text{H}_2\text{O}$ and 5.940 g of $(\text{NH}_4)_2\text{HPO}_4$ were dissolved in 32.288 mL and in 44.06 mL of distilled water, respectively, to prepare homogeneous calcium and phosphate solutions. Then, the pH of the solutions was adjusted to 10 by adding NH_3 . Afterwards, the calcium solution was added (2.4 g/min) over a stirring phosphate solution and stirred for 1 h. The final solution was centrifuged at 5000 rpm for 5 min and, finally, the obtained HAP-NPs were calcined at 500 °C for 5 h.

2.5. Nanoparticle characterization

2.5.1. Transmission electron microscopy and zeta potential analysis

Transmission electron microscopy (TEM) was used to visualize HAP-NPs and determine their dispersion and aggregation status, size, and shape. In this study, for morphological examinations of roundHAP-NPs and rodHAP-NPs a ZEISS brand LEO906 TEM model (Oberkochen, Germany) was used. The zeta potential of nanoparticles was measured to understand their stability and potential interactions in colloidal systems (Rasmussen et al., 2020). Stability measurements of HAP-NPs were performed in a Malvern Zetasizer Nano-ZS.

2.5.2. Fourier transform infrared spectroscopy analysis

Atomic groups have unique fundamental vibrational modes and their peaks in a Fourier Transform Infrared Spectroscopy (FTIR) spectrum represent specific chemical bonds and functional groups (Dee et al., 2002). When molecules are exposed to infrared light, radiation at frequencies matching their fundamental vibrational modes is absorbed. The FTIR spectra show the peak values corresponding to the frequencies

at which the radiation is absorbed and form the fingerprint regions of the measured substance. These regions provide essential information about the synthesis or processing conditions used to obtain synthetic HAP-NPs and help to distinguish it from other types of calcium phosphate. Thus, roundHAP-NPs and rodHAP-NPs were investigated by FTIR spectroscopy using a Bruker-Tensor 27 (Billerica, MA, USA) device at 4 cm^{-1} resolution in transmission mode ranging from 400 to 4000 cm^{-1} .

2.6. *Drosophila* strains and exposure

The Oregon strain of *Drosophila melanogaster* was used for all the experiments except for the wing-spot assay where both, the *multiple wing hair* (*mwh*) and *flare* (*flr*) strains were used (Fig. 1). Initially, a wide range of doses (from 10 to 1000 ppm) was chosen to determine those to be used in the study. Since intense precipitation was observed in the applications of HAP-NPs at 400, 800, and 1000 ppm doses, the highest dose applicable was determined to be 200 ppm. Accordingly, we decided to use four different doses (25, 50, 100, and 200 ppm). Distilled water was used in the reconstitution of the HAP-NPs suspensions and, consequently, it was used as the negative control.

2.7. The *Drosophila* wing somatic mutation and recombination test

The wing somatic mutation and recombination test (SMART) in *Drosophila* was performed according to Graf et al. (1984). To proceed, *mwh/mwh* males were crossed with *flr*³/ln (3LR) *Tm3*, *Bd*⁵ females, and eggs from this cross were collected during 8-h periods. The resulting three-day-old larvae were transferred to test tubes where 4.5 g *Drosophila* Instant Medium were hydrated with 9 mL of 25, 50, 100, and 200 ppm of roundHAP-NPs and rodHAP-NPs dispersions. Larvae were kept in this environment until they became adults. Ethyl-methanesulfonate (EMS, 1 mM) was used as the positive control. Wings

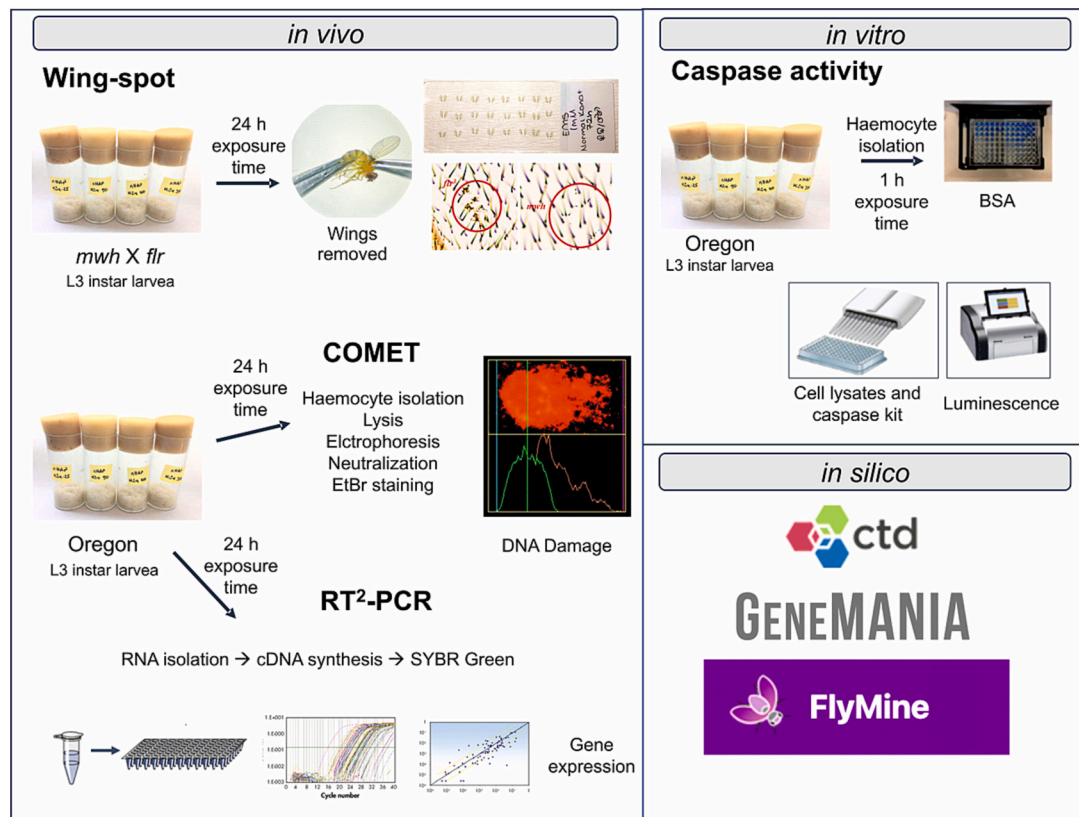


Fig. 1. Scheme of the study. Three different *in vivo* experiments and one *in vitro* experiment were conducted in *D. melanogaster*. Three databases were used for bioinformatic analyses.

were removed from the emerged adults and mounted on microscopy slides with Faure's solution. The wing preparations were analyzed under a light microscope at 40× magnification to detect mutant clones.

2.8. The *Drosophila* single cell gel electrophoresis/comet test

The comet (single cell gel electrophoresis) assay, detecting DNA breaks in larvae hemocytes, was performed according to the [Carmona et al. \(2011\)](#) method. Eight-hour-old eggs were collected from the *Drosophila* Oregon strain to get third instar larvae, which were exposed to 25, 50, 100, and 200 ppm roundHAP-NPs and rodHAP-NPs for 24 h. Distilled water was used as negative control and 4 mM EMS as a positive control. For each dose, 50 cells were counted on a fluorescence microscope (Nikon Eclipse E200, Tokio, Japan) at 40× magnification. The percentage of DNA in the tail was used as the evaluation parameter. All measurements were made with a computer-connected fluorescent microscope and automatic measurement with the COMET Assay-IV (Version 4.11, Instem, UK) software.

2.9. Caspase activity as indicator of apoptosis

To measure caspase activity, 8-h-old eggs were collected from the *Drosophila* Oregon strain. Haemocytes were isolated from 96 h larvae and exposure to HAP-NPs was performed *in vitro*. The Promega Caspase-Glo 3/7, Caspase-Glo 8, and Caspase-Glo 9 Assay (Madison, WI, USA) kits were used to determine caspase activities in *Drosophila* larvae hemocytes. The bicinchoninic acid (BCA) assay was used to determine the amount of protein in the isolated hemocytes. Cell lysates and a caspase kit were added to 96 well plates in a 1:1 ratio (100 µL:100 µL). The plates were mixed for 30 s at 300–500 rpm with the help of a plate-shaker. Afterwards, the plates were incubated for 1 h at room temperature. The amount of luminescence at the end of the time was measured with a multi-module plate reader (Promega Multi Detection System, Madison, USA).

2.10. The gene expression analysis array

The RT² Profiling PCR Array (Qiagen, Hilden, Germany) enables a fast and reliable, allowing to perform faster and more tests than traditional PCR methods. The arrays are pathway-driven panels of the manufacturer's lab-validated qPCR assays with integrated patented controls to ensure a successful experiment every time. Each array in this system can be individually designed and modified to suit unique experimental needs. The human gene homology ratio of the genes whose expression was investigated within the scope of the study was verified by [flybase.org](#). The RT profiles prepared for *Drosophila* gene expressions used the DNA Damage Signaling Pathway PCR Array (Qiagen) in 96-well PCR array plates. It is designed to run two doses in 96-well plates in a panel format. The lowest and highest dose tested in the experiment were used to detect differences in gene activity.

The RT²-PCR study was made as recently published ([Yalcin et al., 2022](#)). Thirty individuals from the treated larvae were collected in microcentrifuge tubes. Total mRNA isolation from larvae was performed using the RNeasy Mini Isolation Kit (Qiagen). After the RNAs were isolated, the amount and quality of RNA was determined using the Nano-drop (Thermo Fisher Scientific, USA) device. After sufficient RNA was isolated, cDNA synthesis was performed with the RT² First Strand Kit. The cDNAs were tested with the RT²-PCR instrument (Applied Biosystems, USA) to determine whether the expression of genes in the DNA damage pathway was altered. A vital advantage of the RT² Profiler PCR Array is the control tests PCR (3 wells), reverse-transcription control (3 wells), and genomic DNA control (1 well). Five wells contain house-keeping genes (*Act42A*, *Gapdh1*, *RpL32*, *SdhA*, and *Tbp*), which are used to calculate normalization in the analysis system. The remaining 36 wells contain genes involved in DNA repair pathways.

2.11. Gene ontology and pathway enrichment analysis

The Gene Ontology Consortium was created by combining information from three model organism databases, FlyBase, Mouse Genome Informatics (MGI), and *Saccharomyces* Genome Database (SGD) ([Ashburner et al., 2000](#)). This system, which provides a basis for the computational analysis of large-scale molecular biology and genetics experiments, has data on >43,000 GO terms, approximately 1,500,000 gene products and >5000 species by 2022. The Comparative Toxicogenomic Database (CTD; <http://ctdbase.org/>) is a digital ecosystem (that holds and can link toxicology data for chemicals, genes, phenotypes, exposures, and related diseases ([Davis et al., 2021](#)). The molecular functions of the 36 genes whose expression was measured were investigated using the gene ontology and pathway enrichment approach.

2.12. Gene-interactions network construction

The GeneMANIA tool finds the genes most closely linked between the networks and selected traits. Thus, GeneMANIA (<http://genemania.org>) is a user-friendly website established to identify the relationships between gene lists and their functions and to generate hypotheses about them ([Warde-Farley et al., 2010](#)). This site has >2000 networks with approximately 164,000 genes and 600 million interactions. Twenty-two genes showing increase and decrease in the RT²-PCR system were added to this database and an estimate was made about the relationship size between them ([Franz et al., 2018](#)).

2.13. The gene pathway Visualizer tool

The [flymine.org](#) is the genomic and proteomic database for *Drosophila* and other insects. This website enables complex queries to be created from a simple scan initiated with one or more data ([Lyne et al., 2007](#)). Over time, this database has been gathered under the umbrella of [intermine.org](#) by combining data from many model organisms, such as *Arabidopsis*, yeast, maggot, mouse, and humans ([Lyne et al., 2022](#)). This gene pathway visualizer has been used to determine the associations involving the selected genes.

2.14. Data analysis

In the *Drosophila* wing SMART test, the statistical analysis of the data was made using the binomial conditional test in the MICROSTA package program. Data from the *Drosophila* comet assay and caspase activities assays were evaluated with the Dunnett' multiple comparison test using analysis of variance (ANOVA) in the IBM SPSS 20 package program. The results of DNA damage signaling pathway PCR array were analyzed using the RT² Profiles PCR Array Data Analysis Software version 3.5. This program calculates fold change/regulation in gene expressions using the delta-delta CT (cycle threshold) method. Delta CT is calculated between the gene of interest (to be measured) and housekeeping genes. Then, Delta-delta CT calculations, Delta CT (Experiment), and Delta CT (control) calculations are made. Fold changes are calculated using the formula $2^{-\Delta\Delta CT}$. The data analysis report is obtained from Qiagen's GeneGlobe web portal. In bioinformatic analysis, the significance of enrichment in molecular functions is calculated by the hypergeometric distribution and adjusted for multiple testing using the Bonferroni method.

3. Results

3.1. Synthesis and characterization

As shown in the TEM images, the synthesized HAP-NPs were round and rod-like ([Fig. 2a, c](#)). The roundHAP-NPs and rodHAP-NPs lengths range from 35 to 60 nm and 45–90 nm, respectively. The Zeta potential demonstrated that the surface charge of roundHAP-NPs was -1.65 mV

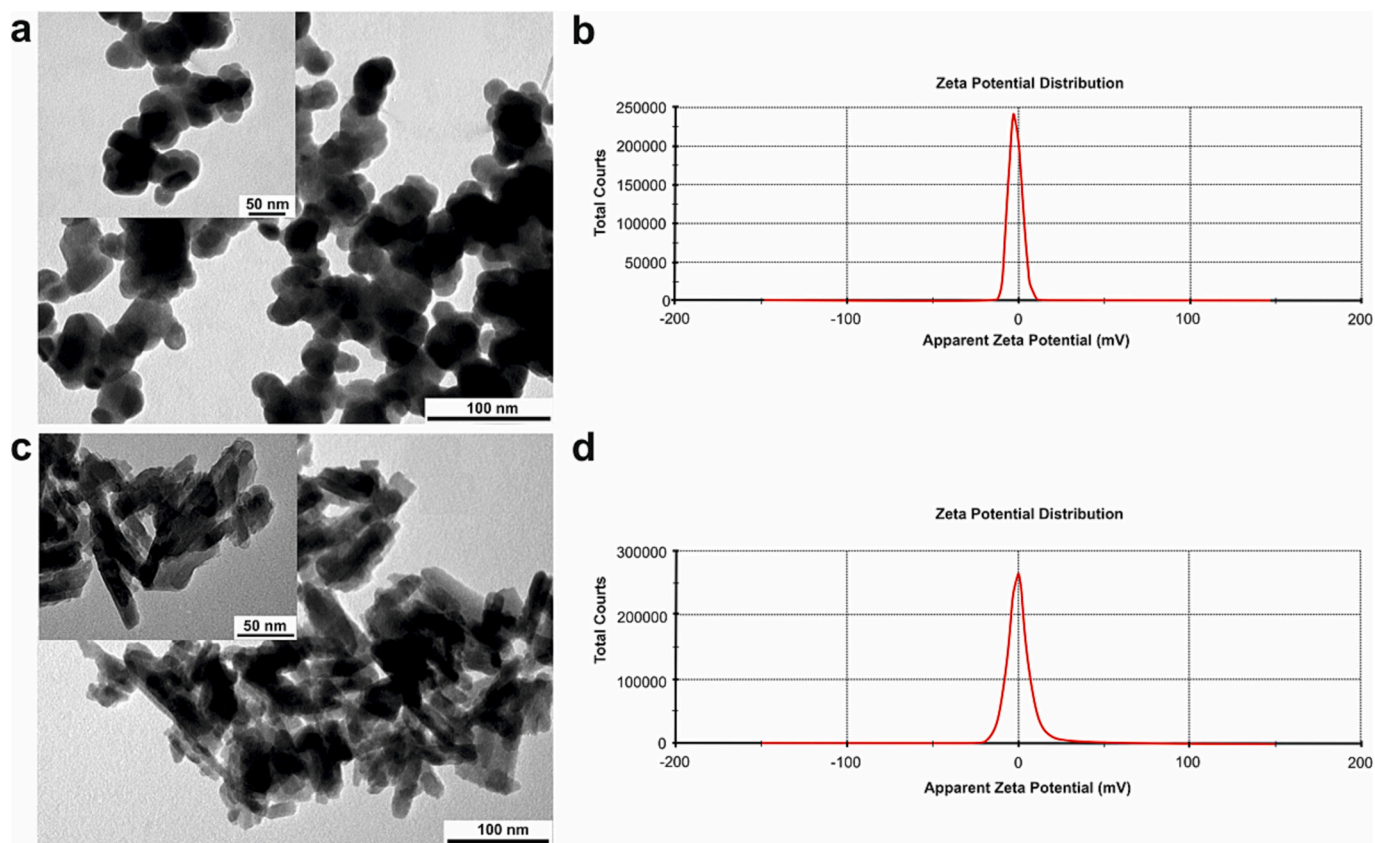


Fig. 2. Characterization of HAP-NPs. TEM images of synthesized HAP-NP and Zeta potential show roundHAP-NPs (a, b) and rodHAP-NPs (c, d).

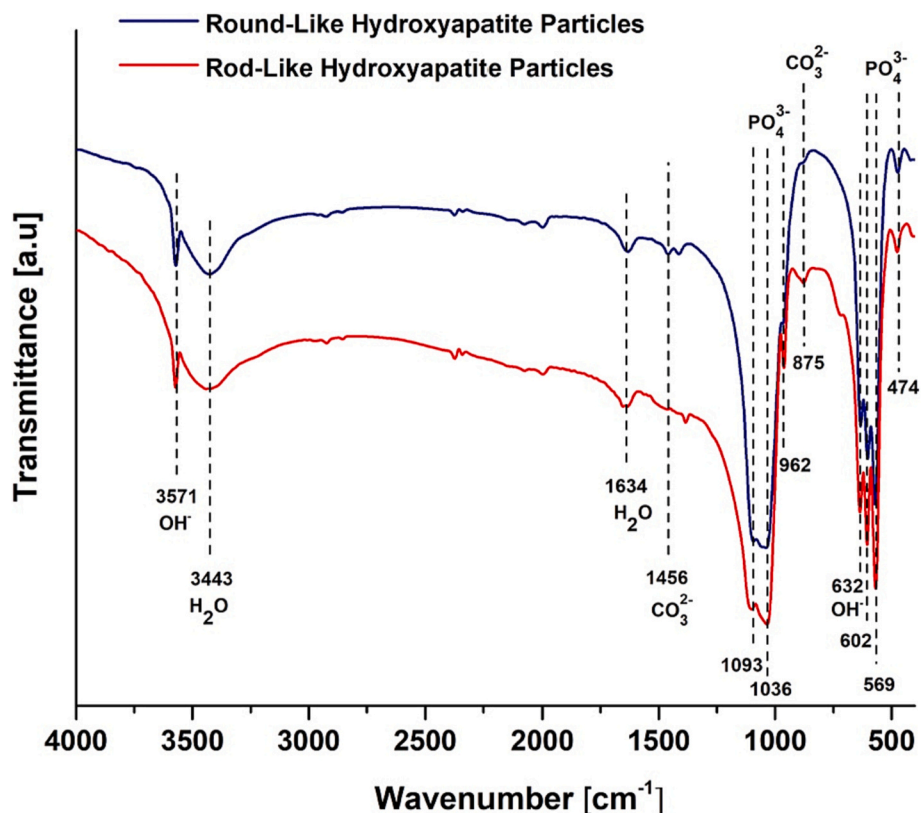


Fig. 3. The FTIR spectra of roundHAP-NPs and rodHAP-NPs.

and rodHAP-NPs 0.37 mV (Fig. 2b, d).

The FTIR spectra for roundHAP-NPs and rodHAP-NPs (Fig. 3) show the functional groups of the obtained HAPs. Typical PO_4^{3-} bands appear at 472, 569, 602, 962, 1036, and 1093 cm^{-1} . The absorbed water (H_2O) is observed in bands at 1634 and 3443 cm^{-1} . The hydroxyl groups (OH^-) in the HAP crystal structure are observed at 632 and 3571 cm^{-1} . The weak carbonate bands (CO_3^{2-}) are observed at 875 and 1456 cm^{-1} . As a summary, the obtained results confirm that both forms of HAP-NPs were effectively synthesized.

3.2. The induction of somatic mutation and recombination

Adult flies were collected from the exposure tubes and kept in tubes containing 70 % ethanol. The analyses were performed by scanning the wings of *Drosophila* individuals to detect changes in the normal morphology of wing hairs. The observed mutant *flr*³ and *mwh* single

spots, as well as the twin spots, were recorded. The obtained results are indicated in Fig. 4, where distilled water and EMS (4 mM) were used as a negative and positive controls, respectively.

According to the results, roundHAP-NPs caused a statistically significant genotoxic effect at 50, 100, and 200 ppm when the frequency of total clones was determined. It should be noted that these effects did not follow a dose-response relationship. As observed, rodHAP-NPs were unable to cause statistically significant genotoxic effects at the studied doses. Representative clone images of the types of mutant spot observed in the wing blade are shown in Fig. 4 (b-e).

3.3. The induction of DNA strand breaks

As observed in Fig. 5, the positive control (4 mM EMS), caused statistically significant DNA damage levels when compared to the negative control group (distilled water), supporting the validity of the reported

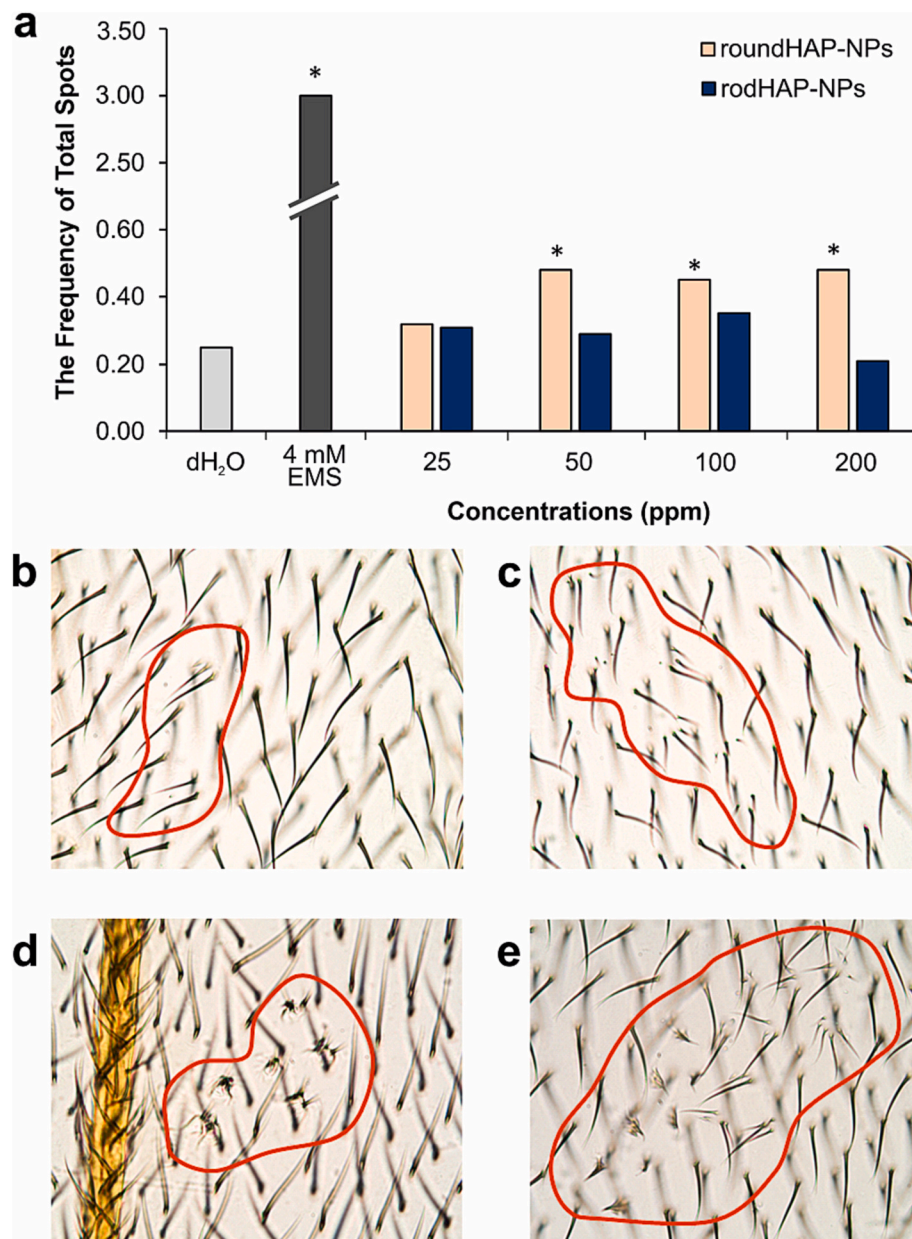


Fig. 4. Genotoxic effects of roundHAP-NPs and rodHAP-NPs on the wings of transheterozygous (*mwh/flr*³) individuals (a). Images of small *mwh* single spot (b), large *mwh* single spot (c), *flr*³ spot (d), and twin spots (e). Distilled water was used as negative control and 1 mM EMS was used as positive control. *P ≤ 0.05 (binomial conditional test).

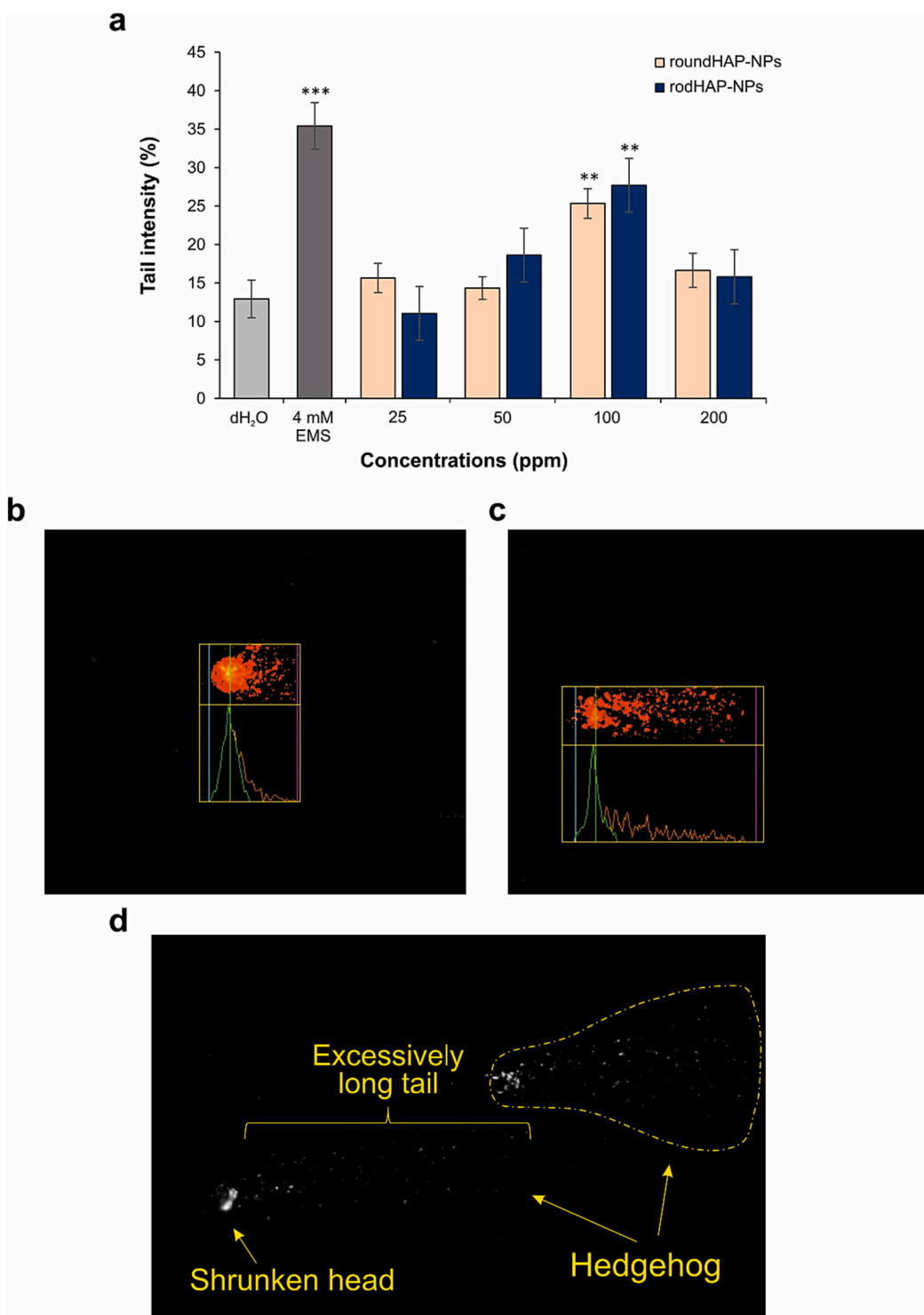


Fig. 5. DNA damage analysis in *Drosophila* hemocytes by using the comet assay. DNA damage induced by roundHAP-NPs and rodHAP-NPs (a). Representative comet images from the negative control (b), the positive control (c), and apoptotic cells (d). * $P \leq 0.05$, ** $P \leq 0.01$, $P \leq 0.001$ (ANOVA, Tukey test).

data. When the effects of roundHAP-NPs were analyzed, a statistically significant DNA damage induction was observed but only at the applied 100 ppm dose (Fig. 5a) ($P < 0.01$). Similar effects were observed when rodHAP-NPs were evaluated since only the dose of 100 ppm induce significant effects ($P < 0.01$). It should be indicated that at the highest dose (200 ppm) many comets with a small and pale head and with almost all the DNA in their tail were observed. These comets, denoted as hedgehog comets are not scored and, consequently, this is the main reason of the lack of significance of the reported data. These figures,

much more present in roundHAP-NPs exposed individuals, have been considered as consequence of apoptotic processes. Undamaged and damaged comet images are given in Fig. 5b-d.

3.4. Caspase activity

The potential induction of apoptosis by roundHAP-NPs and rodHAP-NPs was measured, and the obtained results are indicated in Fig. 6. As observed, roundHAP-NPs at the dose of 100 ppm only induced

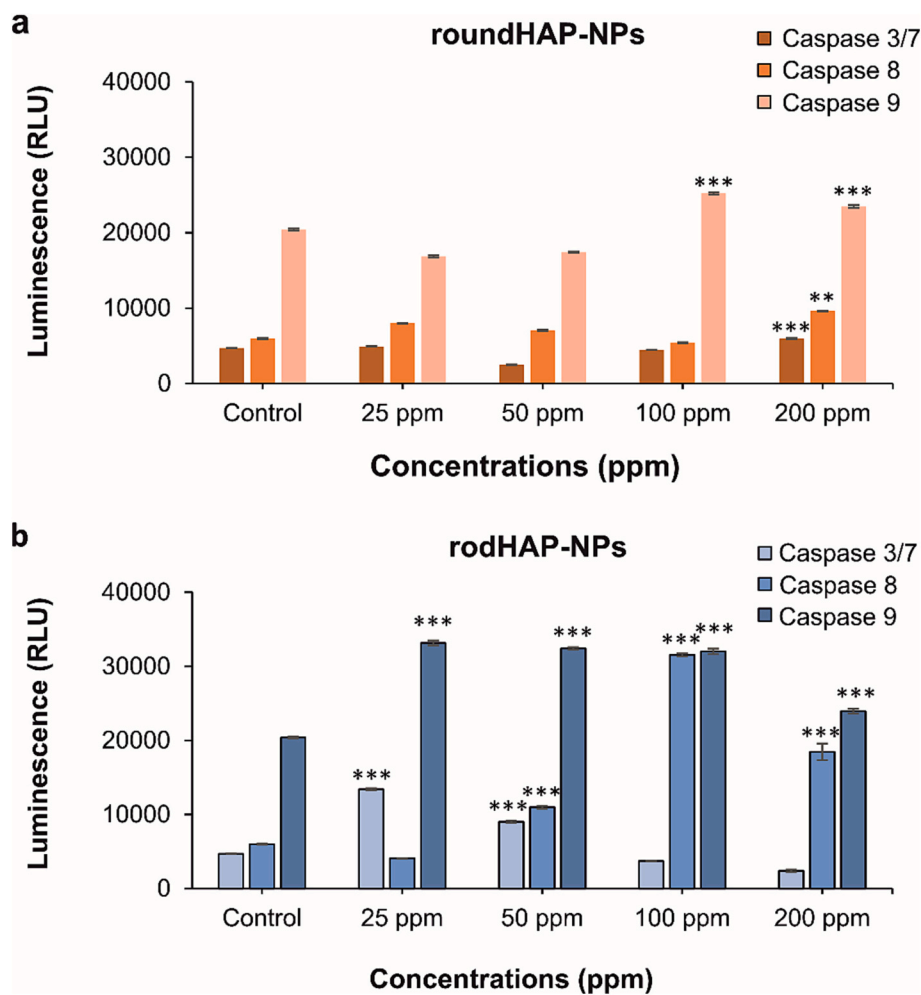


Fig. 6. Results of Caspase-3/7, Caspase-8, and Caspase-9 activities. RoundHAP-NPs (a), rodHAP-NPs (b). *P ≤ 0.05, **P ≤ 0.01, ***P ≤ 0.001 (ANOVA, Tukey test).

statistically significant increases in the activity of caspase-9. At the concentration of 200 ppm the activity of the three caspases (caspase-3/7, caspase-8, and caspase-9) shows statistically significant increases (relatively $P < 0.01$ and $P < 0.001$) (Fig. 6a).

These results show that rodHAP-NPs induced higher effects, as compared with those induced by roundHAP-NPs. Thus, the lowest exposure (25 ppm) increased statistically the activity of caspase-3/7 and caspase-9 and, at the highest concentrations (100 and 200 ppm), caspase-8 and caspase-9 activities increased markedly ($P < 0.001$) (Fig. 6.b).

3.5. Results from the gene expression analysis

The effects of roundHAP-NPs on the expression of the selected genes involved in DNA repair signaling pathways are shown in Table 1. As observed, the *Mlh1* gene is overexpressed in both 25 and 200 ppm treatments, and these effects were statistically significant ($P < 0.05$). Similarly, three other genes (*MCPH1*, *Rad51C*, and *Rad51D*) showed statistically significant decreases after exposures to 25 and 200 ppm of roundHAP-NPs.

Interestingly, the exposure to rodHAP-NPs induced higher levels of changes than those observed after roundHAP-NPs exposure, and most of them involved under-expression. Thus, although no genes reached the established significance levels (fold > 2) at the exposure of 200 ppm, three genes (*mus101*, *Mlh1*, and *Brca2*) were overexpressed at 25 ppm exposure. Regarding the genes showing under-expression, eight were deregulated after exposures to 25 ppm (*PNKP*, *Rev1*, *dap*, *mu2*, *RpLP2*, *Pms2*, *spel1*,

Table 1

Analysis of changes in gene expression levels. Those genes showing increases or decreases with fold changes over 2 are indicated.

	25 ppm			200 ppm				
	▲	FC	▼	FC	▲	FC		
roundHAP-NPs								
<i>Mlh1</i>	3.86		<i>spel1</i>	3.89		<i>Rad51C</i>	4.49	
			<i>Rad51C</i>	4.15		<i>MCPH1</i>	5.92	
<i>Brca2</i>	3.13		<i>MCPH1</i>	8.04	<i>Mlh1</i>	3.32	<i>Rad51D</i>	4.08
			<i>Rad51D</i>	4.32				
rodHAP-NPs								
<i>Mlh1</i>	5.34		<i>PNKP</i>	18.03		<i>spel1</i>	29.79	
<i>Brca2</i>	2.97		<i>Rev1</i>	17.42		<i>dATM</i>	12.88	
			<i>dap</i>	10.94		<i>punt</i>	7.95	
			<i>mu2</i>	10.92		<i>DxpA</i>	7.25	
			<i>RpLP2</i>	6.67		<i>Rev1</i>	6.20	
<i>mus101</i>	2.24		<i>Pms2</i>	6.30		<i>Rad9</i>	6.07	
			<i>spel1</i>	4.73		<i>Rad51D</i>	5.41	
			<i>Sir2</i>	4.22		<i>stg</i>	4.89	
						<i>Hus1-like</i>	4.56	
						<i>Rad17</i>	4.53	
						<i>mu2</i>	4.24	
						<i>Cdk7</i>	4.00	

and *Sir2*) and twelve after exposures to 200 ppm (*spel1*, *dATM*, *punt*, *DxpA*, *Rev1*, *Rad9*, *Rad51D*, *stg*, *Hus1-like*, *Rad17*, *mu2*, and *Cdk7*). Comparing both types of exposures, only three genes were altered at

both doses (*Rev1*, *mu2*, and *spel1*).

3.6. Gene ontology and pathway enrichment

The Gene Ontology (GO) is an extensive bioinformatics database showing species' gene and gene product characteristics. When the molecular functions of the genes involved in the study (Table 2) are examined, it is observed that those involved in catalytic activities and binding to DNA are specially highlighted.

The molecular function of each one of the selected genes can arise from their proteins or RNAs and can consist of a single gene product or a combination of multiple gene products. The table highlights the

importance of the interactions between genes in the management of DNA repair functions. It must be pointed out that >10 % of the genes of the entire genome are involved in the different functions of the DNA repair system, either in the process of recognizing the damage, in cutting the damaged region, or repairing the gaps in the DNA, with the complexes formed by the genes coming together.

3.7. Gene-interaction network construction

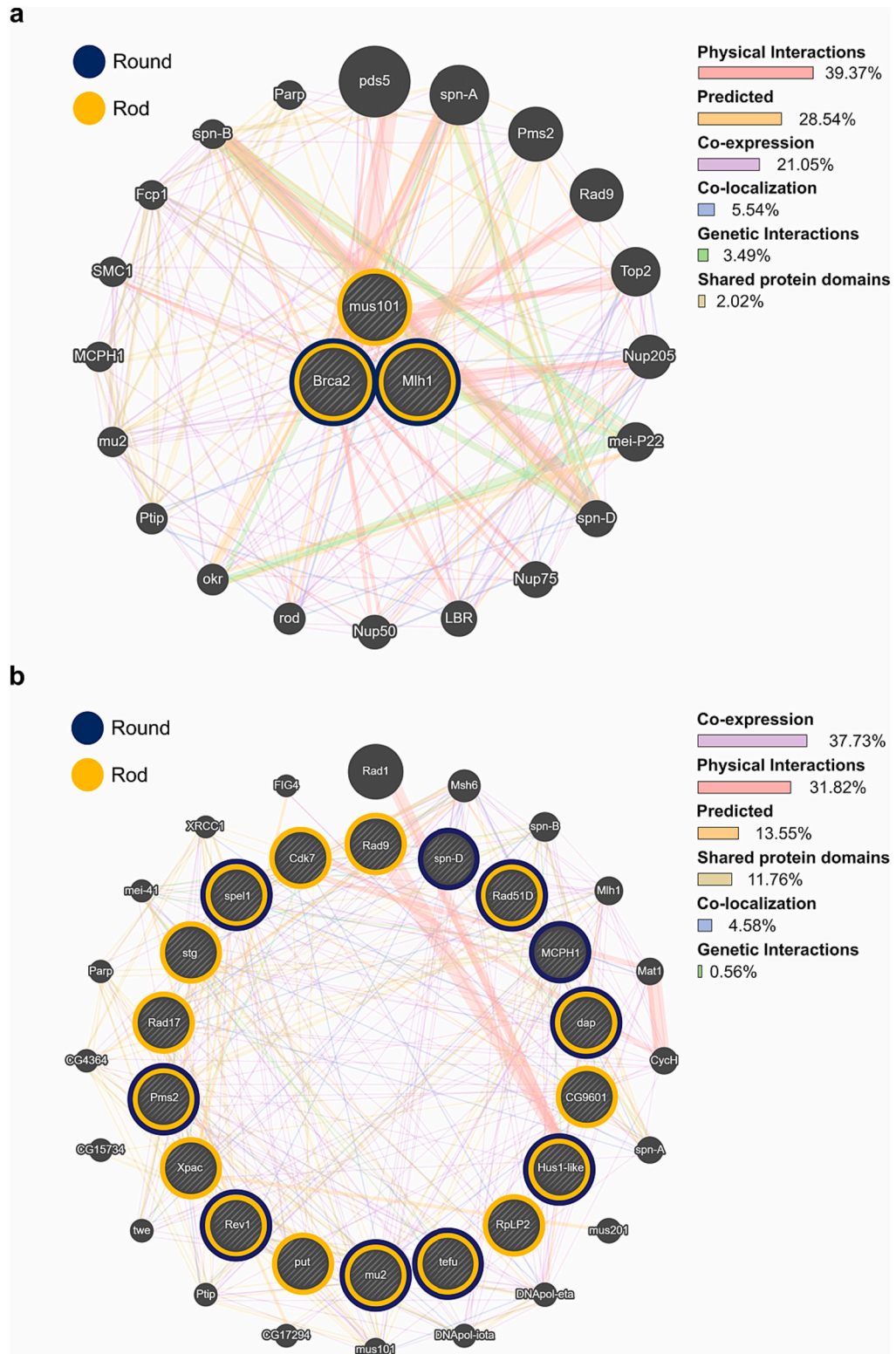
The interactions in the molecular network of the 22 genes showing a statistically significant increase or decrease in the RT²-PCR were determined by using Genemania. Accordingly, 20 genes associated with

Table 2

Molecular functions of the genes involved in this study. A molecular process that can be carried out by the action of a single macromolecular machine, usually via direct physical interactions with other molecular entities. Function in this sense denotes an action, or activity, that a gene product (or a complex) performs (CTD Set Analyzer, <https://ctdbase.org/tools/analyzer.go>, threshold = 0.01).

Highest GO level	GO term name	GO term ID	P-value	Corrected P-value	Annotated genes quantity	Annotated genes	Genome frequency
3	Catalytic activity, acting on DNA	GO:0140097	5.34E-22	7.29E-19	13	CDK7 ERCC1 FEN1 MLH1 OGG1 PCNA PMS2 POLH RAD1 RAD17 RAD50 RAD51D XRCC1	213/45141 genes: 0.47 %
5	Damaged DNA binding	GO:0003684	1.02E-18	1.40E-15	9	ERCC1 FEN1 OGG1 PCNA PNKP POLH RAD1 REV1 XRCC1	65/45141 genes: 0.14 %
2	Catalytic activity, acting on a nucleic acid	GO:0140640	5.47E-17	7.45E-14	13	CDK7 ERCC1 FEN1 MLH1 OGG1 PCNA PMS2 POLH RAD1 RAD17 RAD50 RAD51D XRCC1	514/45141 genes: 1.14 %
4	Nuclease activity	GO:0004518	1.12E-12	1.53E-09	8	ERCC1 FEN1 OGG1 PMS2 PNKP RAD1 RAD50 XRCC1	179/45141 genes: 0.40 %
5	Endonuclease activity	GO:0004519	2.05E-12	2.80E-09	7	ERCC1 FEN1 OGG1 PMS2 PNKP RAD50 XRCC1 BRCA2 ERCC1 FEN1 MLH1 OGG1 PCNA PMS2 PNKP POLH RAD1 RAD50 RAD51D REV1 XRCC1	106/45141 genes: 0.23 %
4	DNA binding	GO:0003677	2.56E-11	3.49E-08	14	BRCA2 ERCC1 FEN1 MLH1 OGG1 PCNA PMS2 PNKP POLH RAD1 RAD50 RAD51D REV1 XRCC1	1799/45141 genes: 3.99 %
4	Deoxyribonuclease activity	GO:0004536	2.79E-10	3.80E-07	5	ERCC1 FEN1 RAD1 RAD50 XRCC1	46/45141 genes: 0.10 %
2	ATP-dependent activity, acting on DNA	GO:0008094	2.79E-10	3.81E-07	6	CDK7 MLH1 PMS2 RAD17 RAD50 RAD51D	110/45141 genes: 0.24 %
3	ATP-dependent DNA damage sensor activity	GO:0140664	1.79E-09	2.45E-06	4	MLH1 PMS2 RAD50 RAD51D	21/45141 genes: 0.05 %
2	DNA damage sensor activity	GO:0140612	3.18E-09	4.34E-06	4	MLH1 PMS2 RAD50 RAD51D	24/45141 genes: 0.05 %
5	Endodeoxyribonuclease activity	GO:0004520	6.12E-09	8.34E-06	4	ERCC1 FEN1 RAD50 XRCC1	28/45141 genes: 0.06 %
3	Nucleic acid binding	GO:0003676	9.49E-09	1.29E-05	14	BRCA2 ERCC1 FEN1 MLH1 OGG1 PCNA PMS2 PNKP POLH RAD1 RAD50 RAD51D REV1 XRCC1	2835/45141 genes: 6.28 %
2	Heterocyclic compound binding	GO:1901363	1.64E-08	2.24E-05	17	BRCA2 CDK7 ERCC1 FEN1 MLH1 OGG1 PCNA PMS2 PNKP POLH RAD1 RAD17 RAD50 RAD51D REV1 SIRT2 XRCC1	4755/45141 genes: 10.53 %
5	Single-stranded DNA binding	GO:0003697	1.72E-08	2.35E-05	5	BRCA2 ERCC1 MLH1 PMS2 RAD51D	103/45141 genes: 0.23 %
2	Organic cyclic compound binding	GO:0097159	2.00E-08	2.72E-05	17	BRCA2 CDK7 ERCC1 FEN1 MLH1 OGG1 PCNA PMS2 PNKP POLH RAD1 RAD17 RAD50 RAD51D REV1 SIRT2 XRCC1	4817/45141 genes: 10.67 %
1	Catalytic activity	GO:0003824	2.09E-08	2.85E-05	17	BRCA2 CDK7 ERCC1 FEN1 MLH1 OGG1 PCNA PMS2 PNKP POLH RAD1 RAD17 RAD50 RAD51D REV1 SIRT2 XRCC1	4832/45141 genes: 10.70 %
6	Single-stranded DNA endodeoxyribonuclease activity	GO:0000014	2.38E-08	3.25E-05	3	ERCC1 RAD50 XRCC1	8/45141 genes: 0.02 %
1	Small molecule sensor activity	GO:0140299	2.44E-08	3.33E-05	4	MLH1 PMS2 RAD50 RAD51D	39/45141 genes: 0.09 %
3	Hydrolase activity, acting on ester bonds	GO:0016788	2.99E-08	4.08E-05	8	ERCC1 FEN1 OGG1 PMS2 PNKP RAD1 RAD50 XRCC1	651/45141 genes: 1.44 %
3	Mismatch repair complex binding	GO:0032404	7.01E-08	9.57E-05	3	MLH1 PCNA PMS2	11/45141 genes: 0.02 %
6	Mismatched DNA binding	GO:0030983	9.35E-08	1.28E-04	3	MLH1 PCNA PMS2	12/45141 genes: 0.03 %
7	3' Overhang single-stranded DNA endodeoxyribonuclease activity	GO:1990599	1.75E-06	0.00239	2	ERCC1 XRCC1	3/45141 genes: 0.01 %
2	Hydrolase activity	GO:0016787	1.98E-06	0.0027	10	ERCC1 FEN1 OGG1 PCNA PMS2 PNKP RAD1 RAD50 SIRT2 XRCC1	2010/45141 genes: 4.45 %
1	ATP-dependent activity	GO:0140657	2.51E-06	0.00342	6	CDK7 MLH1 PMS2 RAD17 RAD50 RAD51D	511/45141 genes: 1.13 %

the 3 genes (*Mlh1*, *Brca2*, *mus101*) showing an increased expression, emerged. These genes show a 39.37 % of physical interaction, a 21.05 % of co-expression, and a 3.49 % of genetic interaction (Fig. 7). In the analysis performed in GeneMANIA, 20 genes were identified as showing associations with the 18 genes which expression was significantly decreased. These genes show 31.82 % physical interaction, 37.73 % co-expression, and 0.56 % genetic interaction.



3.8. Gene pathway visualizer

In Fig. 8, squares represent the genes studied and the circles represent the pathways in which the genes are connected. Pie slices in the circle represent pathways that contain more than one gene. Genes involved in DNA repair are shown in groups. Cell cycle control genes, mismatch repair system genes, nucleotide excision damage detection,

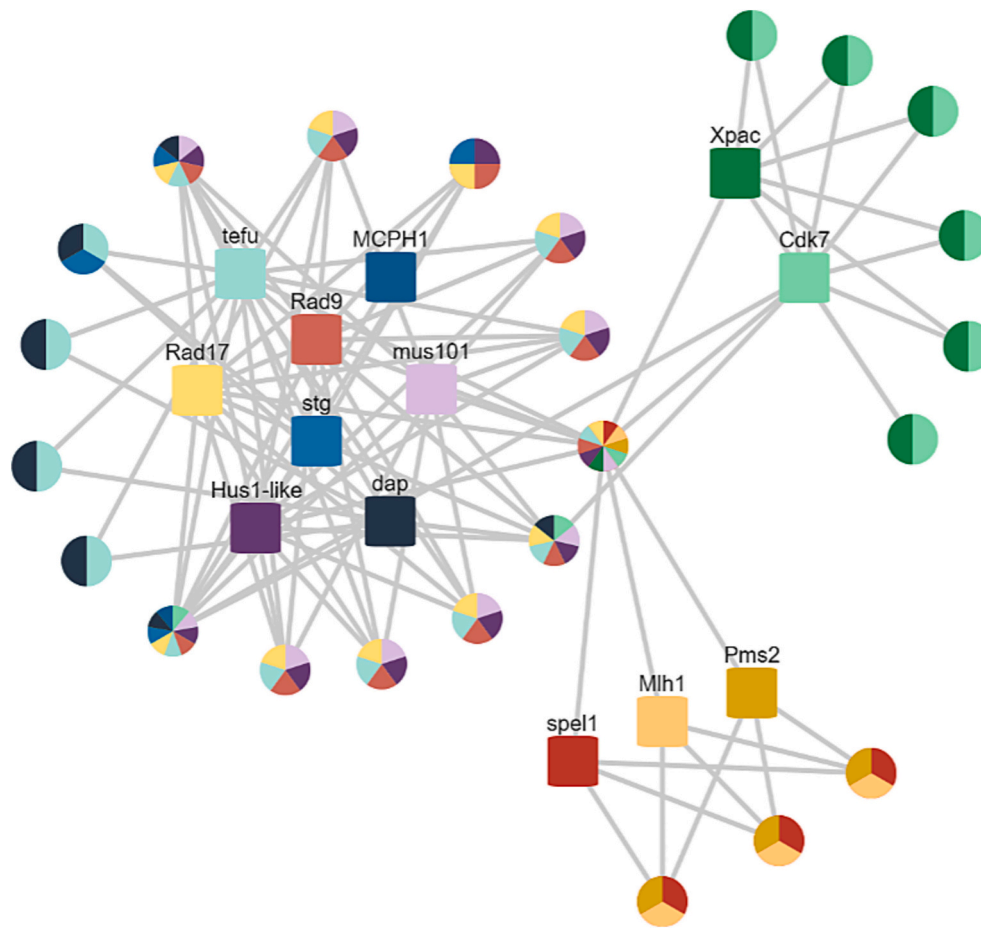


Fig. 8. Gene Pathway Visualizer. Square nodes represent genes. Circular nodes represent pathway annotations for the genes. Edges connect genes and pathways. By default, the most closely related genes and pathways are shown. All genes are involved in DNA repair processes, and some of them are in specialized groups. Thus, *tefu* and *dap* are involved in *tp53*-related pathways, and *tefu*, *dap*, and *stg* are involved in G1/S DNA damage checkpoints. *Spel1*, *mlh1*, and *pms2* are involved in mismatch repair and in the MutSalpha complex-associated mismatch repair. The *xpac* and *cdk7* are included in the NER system together. The *Rad17*, *Rad9*, *mus101*, *Hus1-like*, and *tefu* are involved in double strand repair system.

and apoptosis genes are included in these groupings. Some of the genes are specifically involved in a particular pathway (*Xpac*, *Mlh1*, *Pms2* and *spel1*); but other are involved in multiple pathways, including the cell cycle, repair systems, and apoptotic processes. Thus, *Xpac* and *Cdk7* are involved in the nucleotide excision repair system and work together in the NER system. In addition, *cdk* has a role in the cell cycle. Genes such as *spell1*, *Mlh1* and *Pms2*, involved in the recognition of damage in mismatch repair, work together and have been grouped separately. The genes *dap* and *tefu/dATM* are involved in several steps of DNA repair, particularly in the mechanisms of senescence and apoptosis. *MCPH1*, *dap*, *stg* and *Cdk7* are involved in cell cycle control, while the *Rad* family, *mus101* and *Hus1-like*, are involved in the detection of DNA damage and in the activation of the repair systems.

4. Discussion

In this study, the genotoxic effects of HAP-NPs are discussed at the gene level based in data supported by genotoxicity tests and bioinformatic analyses. Thus, the toxicity of HAP-NPs was comprehensively investigated by *in vitro*, *in vivo*, and *in silico* analyses. Bio-ceramic NPs such as HAP have been used in medicine for a long time, mainly in bone tissue regeneration (Bahadar et al., 2016). Thus, factors such as biocompatibility, interactions with surrounding tissues, and potential toxicity using *in vivo* models have been largely evaluated (Deveci et al., 2020; Ferreira-Ermita et al., 2020). Regarding the few studies carried out using *Drosophila*, roundHAP-NPs exposure was reported to cause behavioral phenotypic disorders in both larvae and adults, as well as oxidative and cell damages (Pappus et al., 2017; Sahu and Mishra, 2020). Nevertheless, no adverse effects such as ROS and lipid peroxidation induction, or alterations in adult climbing and larval crawling

behavior were observed after rodHAP-NPs exposure (Dan et al., 2019). Only one study focuses on the potential genotoxicity of HAP-NPs, showing that resveratrol was able to reduce the genotoxic effects detected by the comet assay; pointing out that oxidatively DNA damage was caused (Turna Demir, 2022). In this context, our study tries to emphasize the potential mechanisms underlying HAP-NPs genotoxicity.

A complete physiochemical characterization of the synthesized HAP-NPs was carried out including Zeta potential, which is a key parameter that indicates the surface charge of nanoparticles, which in turn affects their dispersion and aggregation behavior (Rasmussen et al., 2020). The aggregation observed in the TEM results is correlated with the zeta potential values of the roundHAP-NPs and rodHAP-NPs. In fact, for bone tissue applications it is desired that HAP have a negative or near negative Zeta potential (Doostmohammadi et al., 2012). Furthermore, FTIR results confirmed the efficient synthesis of both rod-like and round-like forms of HAP-NPs (Panda et al., 2003; van der Houwen et al., 2003; Sun et al., 2006; Wang et al., 2006; Lin et al., 2007; Salarian et al., 2009; Ren et al., 2014).

Our results in the wing-spot assay show that exposure to roundHAP-NPs caused significant genotoxic effects in *Drosophila* somatic cells, which not was observed after rodHAP-NPs exposure. It is thought that the genotoxic effects induced by roundHAP-NPs result from their easier cell uptake due to their shape. In addition, this shape has shown to increase oxidative damage in different models (Zhao et al., 2011; Xu et al., 2012). When the comet assay was applied, a significant increase of DNA breaks was observed in the hemocytes of larvae exposed to 100 ppm. Nevertheless, this increase was not observed at the dose of 200 ppm. Interestingly, at this high dose, comets with a small and pale head and with almost all the DNA in their tail were observed. These comets are called “hedgehog” (Collins et al., 2008) and, although initially these

images were associated with apoptosis, further studies proposed that they correspond to one level on a continuum of genotoxic damage, consequently they do not represent a diagnostic of apoptosis (Lorenzo et al., 2013). Independently of the content of the previous discussion about the meaning of the hedgehog comets, the induction of apoptosis can result in a DNA fragmentation with the consequent loss of such fragments during the electrophoresis step. In this way we would explain the non-significant effects observed at the dose of 200 ppm. To determine the potential role played by apoptosis in the observed effects more specific biomarkers must be used.

Caspases are proteins involved in the programmed cell death. In addition, they can regulate various pathological conditions such as neurodegeneration, autoimmune diseases, and cancer (Wu et al., 2016a). Their essential biological role supposes a high conservation over the evolution. Thus, caspases are approximately 50 % conserved between humans and *Drosophila* (Crawford et al., 2012). In *Drosophila*, the initiator caspase DRONC activity, a Caspase-2 and Caspase-9 homologue, is required for developmental and stress-induced apoptosis (Dorstyn and Kumar, 2008). DICER, the *Drosophila* homologue of caspase-3, which acts as an effector caspase, has been associated with developmental apoptosis (Fan and Bergmann, 2010). The high conservation in those genes linked to intrinsic apoptotic pathways suppose that *Drosophila* can be considered as a good model organism for studying the roles of caspases operating during the initiation and implementation of apoptotic cell death. (Fogarty and Bergmann, 2014). The caspase levels in *Drosophila* were investigated after exposures to different agents such as the antibiotic cefotaxime, and cerium and zinc nanoparticles, showing increases in Caspase-3 and Caspase-9 activities (Filipiak et al., 2012; Rahul et al., 2015). In our study, it has been determined that roundHAP-NPs caused an increase in Caspase-3/7 and Caspase-9 activity, and a decrease in Caspase-8 activity. On the other hand, rodHAP-NPs caused a decrease in Caspase-3/7 and Caspase-9 activity, but increased Caspase-8 activity. All this would confirm the induction of intrinsic and extrinsic apoptosis pathways by HAP-NPs exposure (Wu et al., 2016b). According to our results, exposures to low doses of roundHAP-NPs (with high potential to internalize into the cells) can activate intracellular ROS-induced death pathways, while extrinsic apoptotic pathway initiators would be activated at high doses of rodHAP-NPs. The roundHAP-NPs and rodHAP-NPs have similar zeta potential, suggesting that the rate of aggregation is similar in both. These results were also supported by TEM images. The results show that the morphological structure is one of the important factors affecting the toxicity mechanism. These differential roles of the different shapes would agree with the observed by exposing different NPs with different shapes, sizes, and chemical composition (Sohaebuddin et al., 2010).

In eukaryotes, genomic stability is maintained under stress conditions induced by endogenous and exogenous sources. Thus, genomic stability is maintained by DNA repair and cycle checkpoints genes. Major DNA repair pathways are functionally conserved among prokaryotes, primitive and higher eukaryotes, and the proteins involved in these repair processes show a high degree of amino acid identity. With the genome studies, it has been determined that *Drosophila* is one of the model organisms with high similarities (Klovstad et al., 2008). Thus, approximately 77 % of the genes identified in human diseases show homology with *Drosophila* genes (Reiter et al., 2001). In the present study the expression of genes working in nucleotide excision repair, base excision repair, mismatch repair, repair of double-strand breaks, ATM/ATR signaling pathways, and cell cycle checkpoints were investigated in *Drosophila*, as a suitable model organism for investigating DNA damage repair in multicellular organisms. In fact, DNA repair research has its roots in the harmful effects of Muller's X-rays on the *Drosophila* genome, nearly 100 years ago when that pioneering study was published. In our study, thirty-six genes belonging to NER and BER, MMR, double chain breaks repair system, ATM-ATR signaling pathways, cell cycle checkpoints, and apoptosis were analyzed in response to HAP-NPs exposure.

Our results show that the expression of the *Mlh1* gene was increased

at both doses of the roundHAP-NPs, and at the low dose of the rodHAP-NPs, revealing the relevance of that repair pathway. The *Mlh1* gene works in the mismatch repair system to repair point mutations (Sia et al., 2001). As the bioinformatic analysis indicates, *Mlh1* works together with *Pms2* and *spel1* in the mismatch repair pathway. The decrease in these two genes may indicate that this specific repair system does not work properly. On the other hand, the decreased expression of *Rad9* and *Hus1* genes after rodHAP-NPs exposure can be considered as an indicator of DNA damage induction. The complex formed by *Rad9*, *Rad1*, and *Hus1* genes is called "9-1-1" and it is a complex regulating checkpoint signaling pathways after DNA damage (Parrilla-Castellar et al., 2004). Furthermore, it was also determined that the expression of *dap*, *sir2*, and *tefu*, which are involved in apoptotic pathways, decreased after roundHAP-NPs exposure. Caspase results indicate that both intrinsic and extrinsic apoptotic pathways are activated after high exposure doses. Decreased expression of genes suppressing apoptosis and increased caspase activities may point out that roundHAP-NPs exposure induces apoptosis. After exposures to the rodHAP-NPs, the expression of DNA repair genes did not increase statistically, but caspase activities increased. Accordingly, it can be considered that rodHAP-NPs (with a lower potential ability to be internalized), induce apoptosis by causing caspase activities, both in the internal and external pathways. *Brca2*, whose expression is increased in the repair of strand breaks, was over-expressed after low dose exposures. Moreover, Ca ions released from HAP-NPs into the cell could be internalized by the mitochondria causing oxidative stress and apoptosis (Liu et al., 2021; Xia et al., 2022). All this together would indicate that apoptosis can be induced through DNA strand breaks caused by HAP-NP exposures.

As our results show, it is relevant to investigate the toxic potential of different forms of HAP-NPs since the effects can be modulated by their size/shape. This was demonstrated in one study using four different types of HAP-NPs (needle, round, thin rod, and long rod) where a dose-dependent increased in cytotoxicity and apoptosis was observed in rat osteoblast cell lines. In addition, it was observed that the toxic effect occurred mostly in needle-shaped particle exposure, with mild effects in long rod HAP-NP exposures (Xu et al., 2012). This was confirmed by other studies showing that HAP-NPs in short rod and microsphere forms cause increased ROS and DNA damage (comet) in osteoblast primary cells (Dai et al., 2014). In addition, cytotoxicity, ROS, and LDH levels were induced in kidney epithelial cells exposed to different HAP-NPs forms such as spheres, needles, rods, and plates (Rao et al., 2014).

It is assumed that the repair of DNA damage is not carried out by the decrease/increase of a single gene, but by the activation of complex structures that arise with the expression of many genes (Evans et al., 2004; Mannuss et al., 2012). The genes interact with each other in complex pathways and can be controlled by the same transcriptional factors in the same biological pathway, and expected to be functionally similar (Allococo et al., 2004). Although pathways can be studied and analyzed independently, they depend on the expression of interrelated genes. Changes such as mutations in the functions of genes in the hierarchical system may cause changes in the functions of the pathways (Oti and Brunner, 2007; Grimes et al., 2019). The fact that genes responsible for similar functions share features such as interaction with each other and expression patterns has highlighted the term "guilt by association" (GBA) (Gillis and Pavlidis, 2012). GBA has become a phenomenon used to predict genes in certain products or pathways (van Dam et al., 2018), and gene ontology explains the relationships of gene groups in networks with each other by statistically making sense (Gillis and Pavlidis, 2012). In the post-genomic era, data sets in the literature and gene expression analyses by researchers continue defining the interactions between genes and their relationships in the network and constitutes the basis for determining candidate genes in the pathways (Handl et al., 2005; Chiu et al., 2013). Accordingly, to identify the molecular pathways involved is of capital relevance. In such way, bioinformatics analyses permit to identify which genes are working together to repair DNA damage induced, in our case, by HAP-NPs. In this context, the genotoxicity data

obtained in the wing-spot and the comet assays can be better explained when the involved pathways are identified.

Compared to micro-sized HAPs, HAP-NPs have a larger surface area, a higher mechanical strength, and a more bioactive structure. In addition, it binds to the target tissue more effectively both structurally and functionally. HAP-NPs, which releases more Ca, stands out regarding bioactivation in the target tissue (Webster et al., 2000). The Ca release, which is an important feature for biocompatibility, brings along intracellular toxicity problems (Ewence et al., 2008). Size differences is an important factor in assessing the toxicity of nanoparticles (Park et al., 2011; Kaygisiz and Cigerci, 2017; Sukhanova et al., 2018). Although the entry of NPs into the cell varies depending on the cell and particle structure, small-sized particles have a higher potential to cause toxicity because their facility internalize (Augustine et al., 2020). As proved in this study, HAP properties like size, shape, and synthesis time are factor affecting the biological response.

5. Conclusions

In summary, our findings highlight the potential hazardous effects of HAP-NPs in *Drosophila*. This study showed that sol-gel-produced HAP-NPs cause mutations and DNA strand breaks in *Drosophila*. Changes in the expression of genes involved in different DNA repair pathways have been correlated with results in genotoxicity assays. Furthermore, caspase activity increased when apoptosis-suppressed genes decreased. The data obtained in this study are consistent with the literature, as the dimensional and shape differences of nanoparticles may affect the genotoxic potential. In line with the data obtained, the development of new strategies to produce safer HAP-NPs seems to be necessary to improve their clinical applications.

CRediT authorship contribution statement

Bülent Kaya, Nuray Kaya, and Merve Güneş planned the experiments. Esin Akarsu and Emre Yavuz carried out the HA characterization. Merve Güneş, Burçin Yalçın, Ayşen Yağmur Burgazlı, and Ghada Tagorti carried out the rest of the experiments, analyzed the data, carried out the statistical analysis, and prepared tables/figures. Merve Güneş, Bülent Kaya, Nuray Kaya, and Ricard Marcos wrote the final manuscript.

Declaration of competing interest

The authors declare that they have no known competing financial interests or personal relationships that could have appeared to influence the work reported in this paper.

Data availability

Data will be made available on request.

Acknowledgments

This work was supported by the Akdeniz University Scientific Research Projects Coordination Unit [Grant numbers FDK-2019-4457, FBA-2018-3285].

References

Alaraby, M., Annangi, B., Marcos, R., Hernandez, A., 2016. *Drosophila melanogaster* as a suitable *in vivo* model to determine potential side effects of nanomaterials: a review. *J. Toxicol. Environ. Health B* 19 (2), 65–104. <https://doi.org/10.1080/10937404.2016.1166466>.

Allocco, D.J., Kohane, I.S., Butte, A.J., 2004. Quantifying the relationship between co-expression, co-regulation and gene function. *BMC Bioinformatics* 5, (18). <https://doi.org/10.1186/1471-2105-5-18>.

Ashburner, M., Ball, C.A., Blake, J.A., Botstein, D., Butler, H., Cherry, J.M., Davis, A.P., Dolinski, K., Dwight, S.S., Eppig, J.T., Harris, M.A., Hill, D.P., Issel-Tarver, L., Kasarskis, A., Lewis, S., Matese, J.C., Richardson, J.E., Ringwald, M., Rubin, G.M., Sherlock, G., 2000. Gene ontology: tool for the unification of biology. *Nat. Genet.* 25 (1), 25–29. <https://doi.org/10.1038/75556>.

Augustine, R., Hasan, A., Primavera, R., Wilson, R.J., Thakor, A.S., Kevadiya, B.D., 2020. Cellular uptake and retention of nanoparticles: insights on particle properties and interaction with cellular components. *Mater. Today Commun.* 25, 101692 <https://doi.org/10.1016/j.mtcomm.2020.101692>.

Bahadar, H., Maqbool, F., Niaz, K., Abdollahi, M., 2016. Toxicity of nanoparticles and an overview of current experimental models. *Iran. Biomed. J.* 20 (1), 1–11. <https://doi.org/10.7508/ibj.2016.01.001>.

Bonilla-Represa, V., Abalos-Labruzz, C., Herrera-Martinez, M., Guerrero-Perez, M.O., 2020. Nanomaterials in dentistry: state of the art and future challenges. *Nanomaterials-Basel.* 10, (9) <https://doi.org/10.3390/nano10091770>.

Brazdls, R.I., Fieras, I., Avramescu, S.M., Fieras, R.C., 2021. Recent progress in the application of hydroxyapatite for the adsorption of heavy metals from water matrices. *Materials (Basel)* 14 (22), 6898. <https://doi.org/10.3390/ma14226898>.

Carmona, E.R., Guecheva, T.N., Creus, A., Marcos, R., 2011. Proposal of an *in vivo* comet assay using haemocytes of *Drosophila melanogaster*. *Environ. Mol. Mutagen.* 52 (2), 165–169. <https://doi.org/10.1002/em.20604>.

Chiu, W.A., Euling, S.Y., Scott, C.S., Subramanian, R.P., 2013. Approaches to advancing quantitative human health risk assessment of environmental chemicals in the post-genomic era. *Toxicol. Appl. Pharmacol.* 271 (3), 309–323. <https://doi.org/10.1016/j.taap.2010.03.019>.

Collins, A.R., Oscoz, A.A., Brunborg, G., Gaivao, I., Giovannelli, L., Kruszewski, M., Smith, C.C., Stetina, R., 2008. The comet assay: topical issues. *Mutagenesis.* 23 (3), 143–151. <https://doi.org/10.1093/mutage/gem051>.

Crawford, E.D., Seaman, J.E., Barber 2nd, A.E., David, D.C., Babbitt, P.C., Burlingame, A. L., Wells, J.A., 2012. Conservation of caspase substrates across metazoans suggests hierarchical importance of signaling pathways over specific targets and cleavage site motifs in apoptosis. *Cell Death Differ.* 19 (12), 2040–2048. <https://doi.org/10.1038/cdd.2012.99>.

Da, C., Duan, J., Zhang, L., Jia, G., Zhang, C., Zhang, J., 2014. Biocompatibility of defect-related luminescent nanostructured and microstructured hydroxyapatite. *Biol. Trace Elem. Res.* 162 (1–3), 158–167. <https://doi.org/10.1007/s12011-014-0151-0>.

Dan, P., Sundararajan, V., Ganeshkumar, H., Gnanabarathi, B., Subramanian, A.K., Venkatasubu, G.D., Ichihara, S., Ichihara, G., Mohideen, S.S., 2019. Evaluation of hydroxyapatite nanoparticles - induced *in vivo* toxicity in *Drosophila melanogaster*. *Appl. Surf. Sci.* 484, 568–577. <https://doi.org/10.1016/j.apsusc.2019.04.120>.

Davis, A.P., Grondin, C.J., Johnson, R.J., Sciaiky, D., Wiegers, J., Wiegers, T.C., Mattingly, C.J., 2021. Comparative toxicogenomics database (CTD): update 2021. *Nucleic Acids Res.* 49 (D1), D1138–D1143. <https://doi.org/10.1093/nar/gkaa891>.

Dee, K.C., Puleo, D.A., Bizios, R., 2002. *An Introduction to Tissue-biomaterial Interactions: Tissue-Biomaterial*. Wiley-Liss, Inc.

Deveci, M.Z.Y., Gonenc, R., Canpolat, I., Kanat, O., 2020. *In vivo* biocompatibility and fracture healing of hydroxyapatite-hexagonal boron nitride-chitosan-collagen biocomposite coating in rats. *Turk. J. Vet. Anim. Sci.* 44 (1), 76–88. <https://doi.org/10.3906/vet-1906-21>.

Dong, L., Tang, S., Deng, F., Gong, Y., Zhao, K., Zhou, J., Liang, D., Fang, J., Hecker, M., Giesy, J.P., Bai, X., Zhang, H., 2019. Shape-dependent toxicity of alumina nanoparticles in rat astrocytes. *Sci. Total Environ.* 690, 158–166. <https://doi.org/10.1016/j.scitotenv.2019.06.532>.

Doostmohammadi, A., Monshi, A., Salehi, R., Fathi, M.H., Karbasi, S., Pieles, U., Daniels, A.U., 2012. Preparation, chemistry and physical properties of bone-derived hydroxyapatite particles having a negative zeta potential. *Mater. Chem. Phys.* 132 (2–3), 446–452.

Dorstyn, L., Kumar, S., 2008. A biochemical analysis of the activation of the *Drosophila* caspase DRONC. *Cell Death Differ.* 15 (3), 461–470. <https://doi.org/10.1038/sj.cdd.4402288>.

Enax, J., Meyer, F., Schulze Zur Wiesche, E., Epple, M., 2022. On the application of calcium phosphate micro- and nanoparticles as food additive. *Nanomaterials (Basel)* 12 (22), 4075. <https://doi.org/10.3390/nano12224075>.

Epple, M., 2018. Review of potential health risks associated with nanoscopic calcium phosphate. *Acta Biomater.* 77, 1–14. <https://doi.org/10.1016/j.actbio.2018.07.036>.

Evans, M.D., Dizdaroglu, M., Cooke, M.S., 2004. Oxidative DNA damage and disease: induction, repair and significance. *Mutat. Res. Rev. Mutat. Res.* 567 (1), 1–61. <https://doi.org/10.1016/j.mrrev.2003.11.001>.

Ewence, A.E., Bootman, M., Roderick, H.L., Skepper, J.N., McCarthy, G., Epple, M., Neumann, M., Shanahan, C.M., Proudfit, D., 2008. Calcium phosphate crystals induce cell death in human vascular smooth muscle cells a potential mechanism in atherosclerotic plaque destabilization. *Circ. Res.* 103 (5), E28–E34. <https://doi.org/10.1161/Circresaha.108.181305>.

Fan, Y., Bergmann, A., 2010. The cleaved-Caspase-3 antibody is a marker of Caspase-9-like DRONC activity in *Drosophila*. *Cell Death Differ.* 17 (3), 534–539. <https://doi.org/10.1038/cdd.2009.185>.

Ferreira-Ermida, D.A.C., Valente, F.L., Carlo-Reis, E.C., Araújo, F.R., Ribeiro, I.M., Cintra, C.C.V., Borges, A.P.B., 2020. Characterization and *in vivo* biocompatibility analysis of synthetic hydroxyapatite compounds associated with magnetite nanoparticles for a drug delivery system in osteomyelitis treatment. *Results Mater.* 5, 10063. <https://doi.org/10.1016/j.rinma.2020.100063>.

Filip, D.G., Surdu, V.A., Paduraru, A.V., Andronescu, E., 2022. Current development in biomaterials-hydroxyapatite and bioglass for applications in biomedical field: a review. *J. Funct. Biomater.* 13 (4), 248. <https://doi.org/10.3390/jfb13040248>.

Filiplak, M., Tylko, G., Pyza, E., 2012. Zinc induces caspase-dependent mitochondrial pathway of the programmed cell death in haemocytes of *Drosophila melanogaster*. *Biomaterials.* 25 (3), 507–516. <https://doi.org/10.1007/s10534-012-9530-1>.

Fogarty, C.E., Bergmann, A., 2014. Detecting Caspase Activity in Drosophila Larval Imaginal Discs, 1133, pp. 109–117. https://doi.org/10.1007/978-1-4939-0357-3_7.

Franz, M., Rodriguez, H., Lopes, C., Zuberi, K., Montojo, J., Bader, G.D., Morris, Q., 2018. GeneMANIA update 2018. Nucleic Acids Res. 46 (W1), W60–W64. <https://doi.org/10.1093/nar/gky311>.

Furlanetto, M.P., Grivacic, I., Dihl, R.R., Lehmann, M., de Souza, D.S., Plentz, R.D.M., 2018. *In vivo* analysis of photobiomodulation genotoxicity using the somatic mutation and recombination test. Photomed. Laser Surg. 36 (10), 536–540. <https://doi.org/10.1089/pho.2018.4468>.

Gillis, J., Pavlidis, P., 2012. “Guilt by association” is the exception rather than the rule in gene networks. PLoS Comput. Biol. 8 (3), e1002444 <https://doi.org/10.1371/journal.pcbi.1002444>.

Graf, U., Wurgler, F.E., Katz, A.J., Frei, H., Juon, H., Hall, C.B., Kale, P.G., 1984. Somatic mutation and recombination test in *Drosophila melanogaster*. Environ. Mutagen. 6 (2), 153–188. <https://doi.org/10.1002/em.2860060206>.

Grimes, T., Potter, S.S., Datta, S., 2019. Integrating gene regulatory pathways into differential network analysis of gene expression data. Sci. Rep. 9 (1), 5479. <https://doi.org/10.1038/s41598-019-41918-3>.

Handl, J., Knowles, J., Kell, D.B., 2005. Computational cluster validation in post-genomic data analysis. Bioinformatics. 21 (15), 3201–3212. <https://doi.org/10.1093/bioinformatics/bti517>.

Ignjatovic, N.L., Markovic, S., Jugovic, D., Uskokovic, V., Uskokovic, D.P., 2020. From molecules to nanoparticles to functional materials. J. Serb Chem. Soc. 85 (11), 1383–1403. <https://doi.org/10.2298/JSC2004260351>.

Kalpana, M., Nagalakshmi, R., 2023. Nano hydroxyapatite for biomedical applications derived from chemical and natural sources by simple precipitation method. Appl. Biochem. Biotechnol. 195 (6), 3994–4010. <https://doi.org/10.1007/s12010-022-03968-8>.

Kaygisiz, S.Y., Cigerci, I.H., 2017. Genotoxic evaluation of different sizes of iron oxide nanoparticles and ionic form by SMART, Allium and comet assay. Toxicol. Ind. Health 33 (10), 802–809. <https://doi.org/10.1177/0748233717722907>.

Klovstad, M., Abdu, U., Schupbach, T., 2008. *Drosophila brca2* is required for mitotic and meiotic DNA repair and efficient activation of the meiotic recombination checkpoint. PLoS Genet. 4 (2), e31 <https://doi.org/10.1371/journal.pgen.0040031>.

Lin, K.L., Chang, J., Cheng, R.M., Ruan, M.L., 2007. Hydrothermal microemulsion synthesis of stoichiometric single crystal hydroxyapatite nanorods with mono-dispersion and narrow-size distribution. Mater. Lett. 61 (8–9), 1683–1687. <https://doi.org/10.1016/j.matlet.2006.07.099>.

Liu, Q., Xiang, P.P., Chen, M.Y., Luol, Y., Zhao, Y., Zhu, J.Y., Jing, W.W., Yu, H., 2021. Nano-sized hydroxyapatite induces apoptosis and osteogenic differentiation of vascular smooth muscle cells via JNK/c-JUN pathway. Int. J. Nanomedicine 16, 3633–3648. <https://doi.org/10.2147/IJN.S303714>.

Lorenzo, Y., Costa, S., Collins, A.R., Azqueta, A., 2013. The comet assay, DNA damage, DNA repair and cytotoxicity: hedgehogs are not always dead. Mutagenesis. 28 (4), 427–432. <https://doi.org/10.1093/mutage/get018>.

Lyne, R., Smith, R., Rutherford, K., Wakeling, M., Varley, A., Guillier, F., Janssens, H., Ji, W., McLaren, P., North, P., Rana, D., Riley, T., Sullivan, J., Watkins, X., Woodbridge, M., Lilley, K., Russell, S., Ashburner, M., Mizuguchi, K., Micklem, G., 2007. FlyBase: an integrated database for *Drosophila* and *Anopheles* genomics. Genome Biol. 8 (7), R129. <https://doi.org/10.1186/gb-2007-8-7-r129>.

Lyne, R., Bazaga, A., Butano, D., Contrino, S., Heimbach, J., Hu, F.Y., Kalderimis, A., Lyne, M., Reierskog, K., Stepan, R., Sullivan, J., Wise, A., Yehudi, Y., Micklem, G., 2022. HumanMine: Advanced Data Searching, Analysis and Cross-species Comparison, 2022. Database-Oxford. <https://doi.org/10.1093/database/baac054>.

Mannuss, A., Trapp, O., Puchta, H., 2012. Gene regulation in response to DNA damage. Biochim. Biophys. Acta, Gene Regul. Mech. 1819 (2), 154–165. <https://doi.org/10.1016/j.bbagen.2011.08.003>.

Mishra, N., Srivastav, R., Agrawal, U.R., Tewari, R.R., 2017. An insight into the genotoxicity assessment studies in dipterans. Mutat. Res. Rev. Mutat. Res. 773, 220–229. <https://doi.org/10.1016/j.mrrev.2016.10.001>.

Mohd Pu'ad, N.A.S., Koshy, P., Abdullah, H.Z., Idris, M.I., Lee, T.C., 2019. Syntheses of hydroxyapatite from natural sources. Heliyon. 5 (5), e01588 <https://doi.org/10.1016/j.heliyon.2019.e01588>.

Montoya, C., Du, Y., Gianforcaro, A.L., Orrego, S., Yang, M.B., Lelkes, P.I., 2021. On the road to smart biomaterials for bone research: definitions, concepts, advances, and outlook. Bone Res. 9 (1) <https://doi.org/10.1038/s41413-020-00131-z>.

Mosa, I.F., Abd, H.H., Abuzreda, A., Assaf, N., Yousif, A.B., 2020. Bio-evaluation of the role of chitosan and curcumin nanoparticles in ameliorating genotoxicity and inflammatory responses in rats' gastric tissue followed hydroxyapatite nanoparticles' oral uptake. Toxicol. Res. 9 (4), 493–508. <https://doi.org/10.1093/toxres/taaa054>.

Nagyne-Kovacs, T., Studnicka, L., Kincses, A., Spengler, G., Molnar, M., Tolner, M., Lukacs, I.E., Szilagyi, I.M., Pokol, G., 2018. Synthesis and characterization of Sr and mg-doped hydroxyapatite by a simple precipitation method. Ceram. Int. 44 (18), 22976–22982. <https://doi.org/10.1016/j.ceramint.2018.09.096>.

Naves, M.P.C., de Moraes, C.R., Silva, A.C.A., Dantas, N.O., Spano, M.A., de Rezende, A. A.A., 2018. Assessment of mutagenic, recombinogenic and carcinogenic potential of titanium dioxide nanocrystals in somatic cells of *Drosophila melanogaster*. Food Chem. Toxicol. 112, 273–281. <https://doi.org/10.1016/j.fct.2017.12.040>.

Osuchukwu, O.A., Salihu, A., Abdullahi, I., Abdulkareem, B., Nwannenna, C.S., 2021. Synthesis techniques, characterization and mechanical properties of natural derived hydroxyapatite scaffolds for bone implants: a review. SN. Appl. Sci. 3, (10) <https://doi.org/10.1007/s42452-021-04795-y>.

Oti, M., Brunner, H.G., 2007. The modular nature of genetic diseases. Clin. Genet. 71 (1), 1–11. <https://doi.org/10.1111/j.1399-0004.2006.00708.x>.

Pai, S.D., Kini, M.S., Selvaraj, R., 2021. A review on adsorptive removal of dyes from wastewater by hydroxyapatite nanocomposites. Environ. Sci. Pollut. Res. 28 (10), 11835–11849. <https://doi.org/10.1007/s11356-019-07319-9>.

Panda, R.N., Hsieh, M.F., Chung, R.J., Chin, T.S., 2003. FTIR, XRD, SEM and solid state NMR investigations of carbonate-containing hydroxyapatite nano-particles synthesized by hydroxide-gel technique. J. Phys. Chem. Solids 64 (2), 193–199. [https://doi.org/10.1016/S0022-3697\(02\)00257-3](https://doi.org/10.1016/S0022-3697(02)00257-3).

Panda, S., Biswas, C.K., Paul, S., 2021. A comprehensive review on the preparation and application of calcium hydroxyapatite: a special focus on atomic doping methods for bone tissue engineering. Ceram. Int. 47 (20), 28122–28144. <https://doi.org/10.1016/j.ceramint.2021.07.100>.

Pappu, S.A., Ekka, B., Sahu, S., Sabat, D., Dash, P., Mishra, M., 2017. A toxicity assessment of hydroxyapatite nanoparticles on development and behaviour of *Drosophila melanogaster*. J. Nanopart. Res. 19, (4) <https://doi.org/10.1007/s11051-017-3824-8>.

Park, M.V.D.Z., Neigh, A.M., Vermeulen, J.P., de la Fonteyne, L.J.J., Verharen, H.W., Briede, J.J., van Loveren, H., de Jong, W.H., 2011. The effect of particle size on the cytotoxicity, inflammation, developmental toxicity and genotoxicity of silver nanoparticles. Biomaterials. 32 (36), 9810–9817. <https://doi.org/10.1016/j.biomaterials.2011.08.085>.

Parrilla-Castellar, E.R., Arlander, S.J., Karnitz, L., 2004. Dial 9-1-1 for DNA damage: the Rad9-Hus1-Rad1 (9-1-1) clamp complex. DNA Repair (Amst) 3 (8–9), 1009–1014. <https://doi.org/10.1016/j.dnarep.2004.03.032>.

Portugal, J., Mansilla, S., Pina, B., 2022. Perspectives on the use of Toxicogenomics to assess environmental risk. Front. Biosci. 27 (10), 294. <https://doi.org/10.31083/j.fbl2710294>.

Rahul, S.J., Naz, F., Siddique, Y.H., 2015. Evaluation of the toxic potential of cefotaxime in the third instar larvae of transgenic *Drosophila melanogaster*. Chem. Biol. Interact. 233, 71–80. <https://doi.org/10.1016/j.cbi.2015.03.004>.

Rao, P.J., Pelletier, M.H., Walsh, W.R., Mobbs, R.J., 2014. Spine interbody implants: material selection and modification, functionalization and bioactivation of surfaces to improve osseointegration. Optop. Surg. 6 (2), 81–89. <https://doi.org/10.1111/os.12098>.

Rasmussen, M.K., Pedersen, J.N., Marie, R., 2020. Size and surface charge characterization of nanoparticles with a salt gradient. Nat. Commun. 11 (1), 2337. <https://doi.org/10.1038/s41467-020-15889-3>.

Rathanayake, A., Hettithanthori, O., Sandanayake, S., Mahatantila, K., Rajapaksha, A.U., Vithanage, M., 2022. Essence of hydroxyapatite in defluoridation of drinking water: a review. Environ. Pollut. 311, 119882 <https://doi.org/10.1016/j.envpol.2022.119882>.

Reiter, L.T., Potocki, L., Chien, S., Gribskov, M., Bier, E., 2001. A systematic analysis of human disease-associated gene sequences in *Drosophila melanogaster*. Genome Res. 11 (6), 1114–1125. <https://doi.org/10.1101/gr.169101>.

Ren, F.Z., Ding, Y.H., Leng, Y., 2014. Infrared spectroscopic characterization of carbonated apatite: a combined experimental and computational study. J. Biomed. Mater. Res. A 102 (2), 496–505. <https://doi.org/10.1002/jbm.a.34720>.

Righi, S., Prato, E., Magnani, G., Lama, V., Biandolino, F., Parlapiano, I., Carella, F., Iafisco, M., Adamiano, A., 2023. Calcium phosphates from fish bones in sunscreen: an LCA and toxicity study of an emerging material for circular economy. Sci. Total Environ. 862, 160751 <https://doi.org/10.1016/j.scitotenv.2022.160751>.

Sahu, S., Mishra, M., 2020. Hydroxyapatite nanoparticle causes sensory organ defects by targeting the retromer complex in *Drosophila melanogaster*. Nanoimpact 19, 100237. <https://doi.org/10.1016/j.impact.2020.100237>.

Salarian, M., Solati-Hashjin, M., Shafiei, S.S., Salarian, R., Nemati, Z.A., 2009. Template-directed hydrothermal synthesis of dandelion-like hydroxyapatite in the presence of cetyltrimethylammonium bromide and polyethylene glycol. Ceram. Int. 35 (7), 2563–2569. <https://doi.org/10.1016/j.ceramint.2009.02.031>.

Sia, E.A., Dominska, M., Stefanovic, N., Petes, T.D., 2001. Isolation and characterization of point mutations in mismatch repair genes that destabilize microsatellites in yeast. Mol. Cell. Biol. 21 (23), 8157–8167. <https://doi.org/10.1128/MCB.21.23.8157-8167.2001>.

Sohae будин, S.K., Thevenot, P.T., Baker, D., Eaton, J.W., Tang, L., 2010. Nanomaterial cytotoxicity is composition, size, and cell type dependent. Part. Fibre Toxicol. 7, 22. <https://doi.org/10.1186/1743-8977-7-22>.

Sukhanova, A., Bozrova, S., Sokolov, P., Berestovoy, M., Karaulov, A., Nabiev, I., 2018. Dependence of nanoparticle toxicity on their physical and chemical properties. Nanoscale Res. Lett. 13 <https://doi.org/10.1186/s11671-018-2457-x>.

Sun, Y.X., Guo, G.S., Wang, Z.H., Guo, H.Y., 2006. Synthesis of single-crystal HAP nanorods. Ceram. Int. 32 (8), 951–954. <https://doi.org/10.1016/j.ceramint.2005.07.023>.

Turna Demir, F., 2022. Protective effects of resveratrol against genotoxicity induced by nano and bulk hydroxyapatite in *Drosophila melanogaster*. J. Toxicol. Environ. Health, Part A 85 (20), 850–865. <https://doi.org/10.1080/15287394.2022.2101568>.

van Dam, S., Vosa, U., van der Graaf, A., Franke, L., de Magalhaes, J.P., 2018. Gene co-expression analysis for functional classification and gene-disease predictions. Brief. Bioinform. 19 (4), 575–592. <https://doi.org/10.1093/bib/bbw139>.

van der Houwen, J.A.M., Cressey, G., Cressey, B.A., Valsami-Jones, E., 2003. The effect of organic ligands on the crystallinity of calcium phosphate. J. Cryst. Growth 249 (3–4), 572–583. [https://doi.org/10.1016/S0022-0248\(02\)2227-3](https://doi.org/10.1016/S0022-0248(02)2227-3).

Venkatesan, J., Anil, S., 2021. Hydroxyapatite derived from marine resources and their potential biomedical applications. Biotechnol. Bioprocess Eng. 26 (3), 312–324. <https://doi.org/10.1007/s12257-020-0359-0>.

Wang, Y.J., Chen, J.D., Wei, K., Zhang, S.H., Wang, X.D., 2006. Surfactant-assisted synthesis of hydroxyapatite particles. Mater. Lett. 60 (27), 3227–3231. <https://doi.org/10.1016/j.matlet.2006.02.077>.

Warde-Farley, D., Donaldson, S.L., Comes, O., Zuberi, K., Badrawi, R., Chao, P., Franz, M., Grouios, C., Kazi, F., Lopes, C.T., Maitland, A., Mostafavi, S., Montojo, J., Shao, Q., Wright, G., Bader, G.D., Morris, Q., 2010. The GeneMANIA prediction server: biological network integration for gene prioritization and predicting gene function. *Nucleic Acids Res.* 38, W214–W220. <https://doi.org/10.1093/nar/gkq537>.

Webster, T.J., Ergun, C., Doremus, R.H., Siegel, R.W., Bizios, R., 2000. Enhanced functions of osteoblasts on nanophase ceramics. *Biomaterials.* 21 (17), 1803–1810. [https://doi.org/10.1016/S0142-9612\(00\)00075-2](https://doi.org/10.1016/S0142-9612(00)00075-2).

Wu, Y., Zhao, D., Zhuang, J., Zhang, F., Xu, C., 2016b. Caspase-8 and Caspase-9 functioned differently at different stages of the cyclic stretch-induced apoptosis in human periodontal ligament cells. *PLoS One* 11 (12), e0168268. <https://doi.org/10.1371/journal.pone.0168268>.

Wu, Z.H., Yang, S.L., Wu, W., 2016a. Shape control of inorganic nanoparticles from solution. *Nanoscale.* 8 (3), 1237–1259. <https://doi.org/10.1039/c5nr07681a>.

Xia, Y., Li, B., Zhang, F., Wu, Q., Wen, S., Jiang, N., Liu, D., Huang, C., Liu, S., 2022. Hydroxyapatite nanoparticles promote mitochondrial-based pyroptosis via activating calcium homeostasis and redox imbalance in vascular smooth muscle cells. *Nanotechnol.* 33, (27) <https://doi.org/10.1088/1361-6528/ac61ca>.

Xu, Z.L., Liu, C.S., Wei, J., Sun, J., 2012. Effects of four types of hydroxyapatite nanoparticles with different nanocrystal morphologies and sizes on apoptosis in rat osteoblasts. *J. Appl. Toxicol.* 32 (6), 429–435. <https://doi.org/10.1002/jat.1745>.

Yalcin, B., Gunes, M., Kursun, A.Y., Kaya, N., Marcos, R., Kaya, B., 2022. Genotoxic hazard assessment of cerium oxide and magnesium oxide nanoparticles in *Drosophila*. *Nanotoxicol.* 16 (3), 393–407. <https://doi.org/10.1080/17435390.2022.2098072>.

Yavuz, E., Erdem, R., Kucuksayan, E., Akarsu, E., Akarsu, M., 2021. Preparation and characterization of polyethylene glycol functional hydroxyapatite/polycaprolactone electrospun biomembranes for bone tissue engineering applications. *Fiber Polym.* 22 (5), 1274–1284. <https://doi.org/10.1007/s12221-021-0560-6>.

Zaffarin, A.S.M., Ng, S.F., Ng, M.H., Hassan, H., Alias, E., 2021. Nano-hydroxyapatite as a delivery system for promoting bone regeneration in vivo: a systematic review. *Nanomaterials-Basel.* 11, (10) <https://doi.org/10.3390/nano11102569>.

Zhao, X., Heng, B.C., Xiong, S., Guo, J., Tan, T.T., Boey, F.Y., Ng, K.W., Loo, J.S., 2011. *In vitro* assessment of cellular responses to rod-shaped hydroxyapatite nanoparticles of varying lengths and surface areas. *Nanotoxicol.* 5 (2), 182–194. <https://doi.org/10.3109/17435390.2010.503943>.

Zhao, X., Ong, K.J., Ede, J.D., Stafford, J.L., Ng, K.W., Goss, G.G., Loo, S.C., 2013. Evaluating the toxicity of hydroxyapatite nanoparticles in catfish cells and zebrafish embryos. *Small* 9 (9–10), 1734–1741. <https://doi.org/10.1002/smll.201200639>.